nature photonics

LETTERS

PUBLISHED ONLINE: 15 MARCH 2009 | DOI: 10.1038/NPHOTON.2009.25

All-optical high-speed signal processing with silicon–organic hybrid slot waveguides

C. Koos[1†], P. Vorreau[1], T. Vallaitis[1], P. Dumon[2], W. Bogaerts[2], R. Baets[2], B. Esembeson[3], I. Biaggio[3], T. Michinobu[4], F. Diederich[4], W. Freude[1*] and J. Leuthold[1*]

Integrated optical circuits based on silicon-on-insulator technology are likely to become the mainstay of the photonics industry. Over recent years an impressive range of silicon-on-insulator devices has been realized, including waveguides[1,2], filters[3,4] and photonic-crystal devices[5]. However, silicon-based all-optical switching is still challenging owing to the slow dynamics of two-photon generated free carriers. Here we show that silicon–organic hybrid integration overcomes such intrinsic limitations by combining the best of two worlds, using mature CMOS processing to fabricate the waveguide, and molecular beam deposition to cover it with organic molecules that efficiently mediate all-optical interaction without introducing significant absorption. We fabricate a 4-mm-long silicon–organic hybrid waveguide with a record nonlinearity coefficient of $\gamma \approx 1 \times 10^5\ \mathrm{W^{-1}\,km^{-1}}$ and perform all-optical demultiplexing of 170.8 Gb s^{-1} to 42.7 Gb s^{-1}. This is—to the best of our knowledge—the fastest silicon photonic optical signal processing demonstrated.

Silicon processing technology has developed to the extent that millimetre-scale devices are routinely fabricated with nanometre precision in modern high-volume complementary metal-oxide–semiconductor (CMOS) lines. This mature technology has now also made silicon-on-insulator (SOI) an attractive platform for photonic integration. Being transparent at infrared telecommunication wavelengths, silicon is suitable for use in passive linear devices. For active devices, such as on-chip lasers and amplifiers, the indirect bandgap of silicon presents an obstacle and has to be overcome, either by making use of Raman amplification[6,7] or by bonding III–V heterostructures onto SOI waveguides. The latter technique enables fabrication of electrically pumped amplifiers[8], continuous-wave (c.w.) lasers[9,10], mode-locked lasers[11] and photodetectors[12].

However, there are other optical functionalities, in particular nonlinear ones, that cannot be realized easily when relying only on the intrinsic properties of silicon. Second-order optical nonlinearities are absent in unstrained bulk silicon because of its centrosymmetry, so recent high-speed modulators are based on free-carrier injection, allowing for transmission speeds of up to 40 Gb s^{-1} (ref. 13). Third-order nonlinearities, which enable all-optical switching and wavelength conversion, are present in silicon, but functionality is limited by two-photon absorption (TPA) and speed limitations due to TPA-induced free-carrier absorption (FCA). Maximum data rates of 10 Gb s^{-1} have been demonstrated in bare silicon waveguides[14], and 40 Gb s^{-1} have been achieved[15] by using a reverse-biased p–i–n diode for removing the generated carriers.

To achieve higher processing speeds, silicon may be combined with another material that has a fast electronic third-order nonlinearity. Located just above silicon on the periodic table is the carbon atom, which can generate a multitude of compounds characterized by large delocalized electron systems. Pioneering experiments[16] have shown that optical polymers allow single-frequency modulation speeds in the terahertz range. However, the coexistence of slow and fast nonlinear dynamics has hindered ultrafast processing of broadband communication signals up to now.

Here we present the first experimental proof of ultrafast communication signal processing using silicon-based devices for transmission speeds above 100 Gb s^{-1}. The inherent limitations of silicon are overcome by using a silicon–organic hybrid (SOH) approach. In particular, we demonstrate an ultrahigh nonlinearity coefficient $\gamma \approx 1 \times 10^5\ \mathrm{W^{-1}\,km^{-1}}$ in slotted SOH waveguides, confirming experimentally, for the first time, the record values predicted by theory[17]. We are also able to prove that FCA losses do not arise in SOH waveguides and therefore do not impose a speed limitation. The concept of SOH integration can also be applied to electro–optic devices[18–21].

The SOH waveguide structure is shown in Fig. 1a. It consists of a silicon slotted waveguide that is filled and surrounded by a nonlinear organic cladding[21,22]. Key to the device's highly nonlinear ultrafast performance is a combination of three unique advantages. First, the organic material can be developed independently from the silicon waveguide to obtain optimum nonlinear optical properties. It can be highly $\chi^{(3)}$-nonlinear without suffering from TPA and associated FCA. Second, the silicon waveguide can be optimized essentially independently from the organic material. A slotted geometry can be chosen to provide maximum electric field magnitude inside the slot. Third, using quasi-transverse-electric (quasi-TE) polarization, the electric field is enhanced in the organic material owing to the electromagnetic boundary conditions at the interface between the high-refractive-index silicon and the low-refractive-index organic. The enhancement of the horizontal field (E_x) is equal to a factor $(n_{\mathrm{Si}}/n_{\mathrm{organic}})^2 = 4$ for $n_{\mathrm{organic}} = 1.8$ and $n_{\mathrm{Si}} = 3.5$ (see Fig. 1a).

To maximize the nonlinearity coefficient $\gamma = (n_2 k_0)/A_{\mathrm{eff}}^{(3)}$, where k_0 is the free-space wavenumber and n_2 the nonlinear refractive index (optical Kerr coefficient) of the cladding, the smallest possible effective area of nonlinear interaction $A_{\mathrm{eff}}^{(3)}$ is required. Calculations[17] show that $A_{\mathrm{eff}}^{(3)}$ can be smaller than 0.1 μm^2 for our cladding material with refractive indices $n_{\mathrm{organic}} < 2$. Waveguides consisting only of the low-index organic material would be much more difficult to fabricate and cannot provide a comparable field concentration.

The SOH structure was obtained by first producing the SOI slot waveguide and then covering it by vapour deposition of highly nonlinear organic molecules. The slotted waveguides were produced on a 200-mm CMOS line using 193-nm deep-ultraviolet (DUV)

[1]Institute of Photonics and Quantum Electronics, University of Karlsruhe, 76131 Karlsruhe, Germany, [2]Photonics Research Group, Ghent University – IMEC, B-9000 Gent, Belgium, [3]Department of Physics and Center for Optical Technologies, Lehigh University, Bethlehem, Pennsylvania 18015, USA, [4]Laboratorium für Organische Chemie, ETH Zürich, Hönggerberg, HCI, CH-8093 Zürich, Switzerland. †Present address: Carl Zeiss AG, Corporate Research and Technology, 73447 Oberkochen, Germany. *e-mail: w.freude@ipq.uka.de; j.leuthold@ipq.uka.de

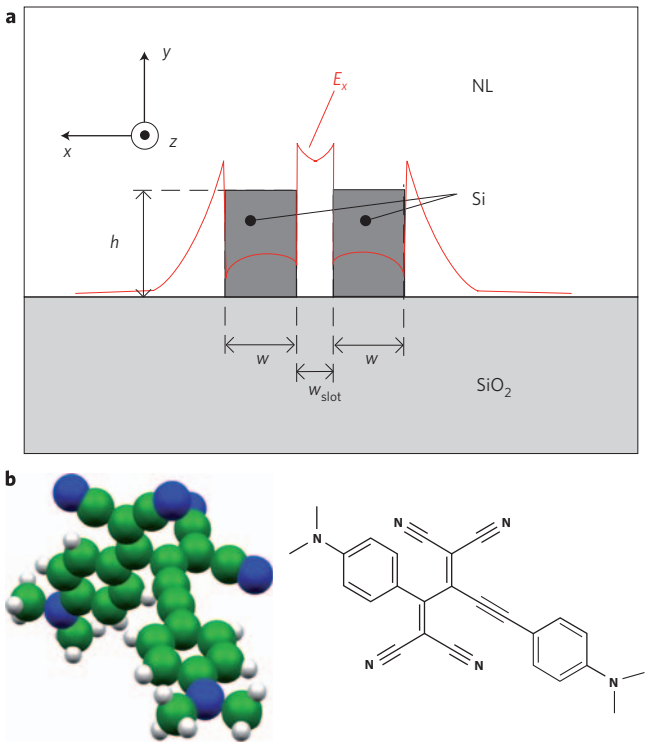

Figure 1 | Structure and organic molecule of a SOH slot waveguide. **a**, Schematic of the waveguide cross-section comprising two silicon ribs on a silicon dioxide buffer layer covered by a nonlinear optical organic material (NL). The quantities *w* and *h* denote the width and the height of the ribs, and w_{slot} is the slot width. For the fundamental quasi-TE mode, the dominant (horizontal) electric field component E_x (depicted in red) is strongly enhan-ced within the low-index material filling the slot. **b**, Molecular structure of the vapour-deposited small molecule DDMEBT[23].

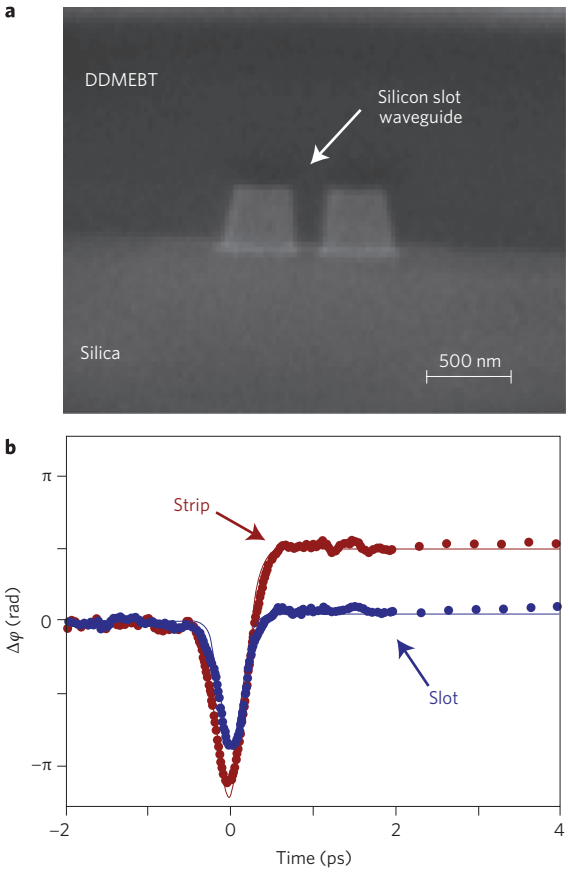

Figure 2 | Scanning electron microscope (SEM) image of the SOH waveguide and nonlinear waveguide dynamics. **a**, SEM image of the cross-section of the vapour-deposited organic film covering the silicon waveguide. The ability of the organic material to homogeneously fill the slot between the waveguides is a key feature of the organic cover layer and of its deposition process. **b**, Nonlinear phase dynamics of the SOH slot waveguide and of a SOH strip waveguide. The slot waveguide has an ultrafast response, whereas the strip waveguide shows the slow phase dynamics caused by TPA-generated free carriers. Dots represent measured values; thin solid line is fitted.

lithography and chlorine-based reactive ion etching[4]. The thickness of the SOI device layer (waveguide height) was $h = 220$ nm, and the buried oxide was 2 μm thick.

To deposit the organic cladding material, spin-coating can be used[18]. However, for third-order nonlinear interaction, the propagation loss is crucial to the functionality of the device, so it is of paramount importance to homogeneously fill the narrow slot with the organic material. We therefore used molecular beam deposition of a small molecule, DDMEBT[23] (2-[4-(dimethylamino)phenyl]-3-{[4-(dimethylamino)phenyl]ethynyl}buta-1,3-diene-1,1,4,4-tetracarbonitrile) to fabricate the organic cladding. The DDMEBT molecule has a non-planar geometry (shown in Fig. 1b) that promotes the formation of an amorphous supramolecular assembly without any grains or inhomogeneities. DDMEBT is part of a family of molecules with a third-order polarizability that is extraordinarily large in relation to the size of the molecule[23–25]. The organic film was ~950 nm thick, flat to the nanometre scale, and featured a large isotropic, off-resonant Kerr coefficient $n^2 \approx (1.7 \pm 0.8) \times 10^{-17}$ m^2 W^{-1} at a wavelength of 1.5 μm (ref. 23). The linear refractive index was $n = 1.8 \pm 0.1$. As can be seen in Fig. 2a, the cover layer homogeneously surrounds the waveguides, and perfectly fills the slot without forming any voids. This is probably due to the mobility of the molecules on the substrate during deposition. The high optical quality of the organic cladding is confirmed by the fact that it does not significantly affect the linear propagation loss of SOH waveguides. (See Methods for more details.)

The nonlinearity parameter γ of the SOH waveguide was obtained by measuring the conversion efficiency $\eta \propto (\gamma L_{eff})^2$ of partially degenerate four-wave mixing with a c.w. pump and signal. The quantity L_{eff} is the effective waveguide length accounting for both linear waveguide loss and group-velocity dispersion. For different samples with nominally identical geometry, we measured[26] values between $\gamma = 104{,}000$ and 83,000 W^{-1} km^{-1}, which is much larger than for holey fibres[27] ($\gamma = 1{,}860$ W^{-1} km^{-1}) and larger than for silicon–polymer strip waveguides[16] ($\gamma = 40{,}000$ W^{-1} km^{-1}) or chalcogenide fibres[28] ($\gamma = 68{,}000$ W^{-1} km^{-1}). (See Methods for more details.)

The nonlinear organic cladding in SOH shows an instantaneous Kerr-type response without impairment by TPA and FCA. To prove this, we compared the SOH slot waveguide of Fig. 1a with a simple DDMEBT-covered silicon strip, in which the quasi-TE mode is concentrated in the silicon core. With heterodyne pump-probe measurements[29,30] we showed that SOH slot waveguides are indeed dynamically superior to SOH strip waveguides (see Methods). Figure 2b shows the ultrafast phase response of the SOH slot waveguide, and for the SOH strip a slowly decaying phase shift of opposite sign. This is due to TPA-generated free carriers with a carrier lifetime of $\sim 1.2 \pm 0.1$ ns. Although bare silicon strip waveguides can exhibit strong nonlinearities[14,17] ($\gamma > 100{,}000$ W^{-1} km^{-1}), free-carrier dynamics on this timescale lead to severe pattern effects in high-speed signal processing.

Finally, to prove the viability of SOH slot waveguides for all-optical processing of broadband telecommunication signals by four-wave mixing (FWM), we demonstrate demultiplexing of a 170.8 Gb s^{-1} return-to-zero (RZ) datastream to a bit rate of

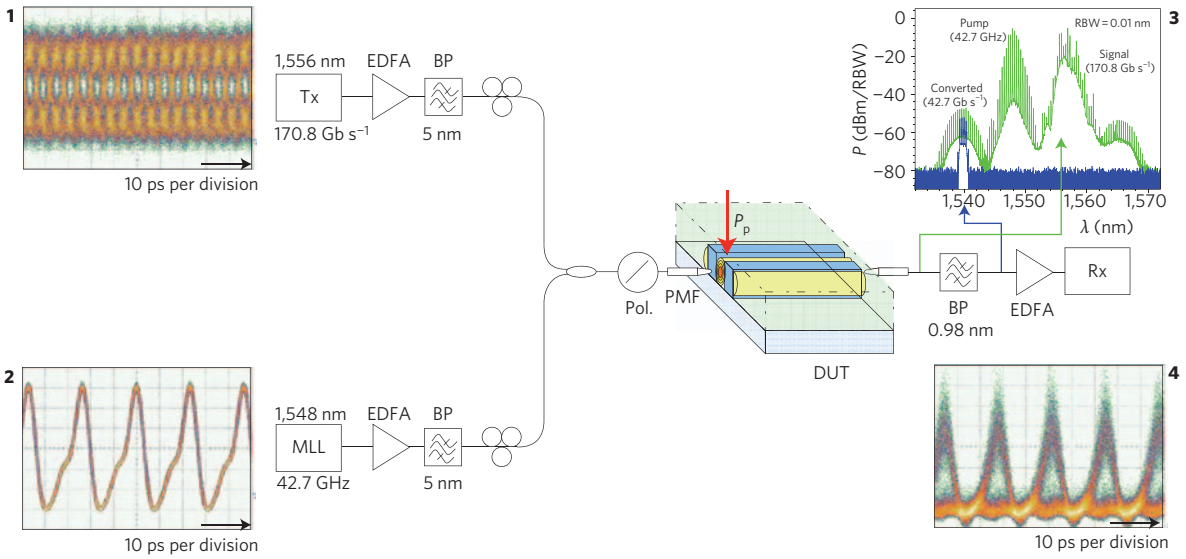

Figure 3 | Experimental set-up of the all-optical demultiplexing by four-wave mixing. Tx indicates a 170.8 Gb s^{-1} transmitter, comprising a 42.7 GHz mode-locked laser, a data modulator, an optical time-division multiplexer, and an optical delay line for synchronization. MLL indicates a mode-locked laser, EDFA an erbium-doped fibre amplifier, BP an optical bandpass filter, Pol a polarizer, PMF a polarization-maintaining fibre, DUT a device under test, Rx a receiver comprising a 120 GHz photodiode and a digital communication analyser, and RBW the resolution bandwidth. Insets: **1**, eye diagram of the 170.8 Gb s^{-1} data signal; **2**, eye diagram of the 42.7 GHz pump; **3**, the spectrum at the output of the DUT (green) and after bandpass-filtering (blue); **4**, eye diagram of the demultiplexed 42.7 Gb s^{-1} signal.

42.7 Gb s^{-1}. The set-up of Fig. 3 comprises two synchronized mode-locked fibre lasers for data and pump, both operating at repetition rates of 42.7 GHz and emitting pulses of ~3 ps full-width at half-maximum (FWHM). The 170.8 Gb s^{-1} data stream is generated by modulating the 42.7 GHz pulse train with a pseudo-random bit sequence ($2^{31}-1$ bit), and by subsequent optical time-division multiplexing; see inset 1, Fig. 3 (eye diagram). Owing to the limited electronic receiver bandwidth, the eye diagram is distorted. Signal and pump (inset 2, Fig. 3) are amplified and coupled into an SOH slot waveguide (height $h = 220$ nm, strip width $w = 212$ nm, slot width $w_{slot} = 205$ nm, length $L = 4.0$ mm). The output signal is bandpass-filtered at the converted wavelength, amplified and detected; see inset 3, Fig. 3, for the optical spectra. There is no leakage through the filter at the pump and signal wavelengths; see Methods. Inset 4, Fig. 3 depicts the demultiplexed signal's eye diagram for an average on-chip pump power of $P_p = 16.6$ dBm (48 mW). (See Methods for more details.)

In summary, we have fabricated and characterized SOH slot waveguides using DUV lithography, standard CMOS processing, and organic molecular beam deposition. We obtained record nonlinearities of about 1×10^5 W^{-1} km^{-1} in the 1.55 μm telecommunication window. By using FWM we demultiplexed a 170.8 Gb s^{-1} telecommunication signal to 42.7 Gb s^{-1}. In view of the potential for improving fibre-chip coupling as well as waveguide loss and waveguide geometry, this is a key step towards complex silicon-based photonic integrated circuits.

Methods

Waveguide fabrication. DUV lithography at 193 nm was performed on an ASML PAS5500/1100 stepper. The organic cladding was deposited in high vacuum at a pressure of 10^{-6} mbar. Powder made of the organic material was heated to 130 °C to generate a molecular beam directed onto the substrate. The growth rate amounted to ~1 nm per minute.

Using atomic force microscope (AFM) scans of the surface, we found that it was flat to the nanometre scale over micrometre lengths[23]. In addition, we took a series of SEM images while slicing the slot waveguide with a Carl Zeiss CrossBeam (focused-ion beam, FIB) system at several positions parallel and perpendicular to the waveguide axis (a perpendicular cut similar to that in Fig. 2a). No grains or voids were found.

For characterization of the slot waveguides, TE-polarized light (the dominant electric field component parallel to the substrate plane) was launched to and detected from the cleaved waveguide facets using polarization-maintaining lensed fibres. A cut-back method was applied to measure the wavelength-dependent loss of the slot waveguides and the fibre-to-chip coupling loss. For a waveguide of height $h = 220$ nm, width $w = 216$ nm and a slot width of $w_{slot} = 157$ nm, the propagation loss was $\alpha_{dB} = 1.6$ dB mm^{-1} ($\alpha = 0.37$ mm^{-1}) at a wavelength of 1,550 nm, and the corresponding fibre-to-chip coupling loss was $a_{cp} = 6.2$ dB per facet. For a reference waveguide with identical geometry but covered with SiO_2, the propagation loss was 1.2 dB cm^{-1} and was therefore only slightly smaller than for the DDMEBT-covered waveguide. The absence of strong scattering loss confirmed the good optical homogeneity of the DDMEBT film.

Characterization of nonlinearities. For a waveguide of geometrical length L and nonlinearity parameter γ, the conversion efficiency for degenerate FWM with c.w. signal and pump waves is given by

$$\eta = \exp(-\alpha L)\left(\gamma P_p L_{eff}\right)^2 \quad (1)$$

where P_p denotes the on-chip pump power just after the input facet of the waveguide and α is the linear propagation loss coefficient. The effective waveguide length $L_{eff} < L$ accounts for both linear propagation loss and group velocity dispersion (GVD) and is given by

$$L_{eff} = \sqrt{1+\exp(-2\alpha L)-2\exp(-\alpha L)\cos(\Delta\beta L)}\Big/\sqrt{\alpha^2+\Delta\beta^2}$$
$$\Delta\beta = \pi c D_2 \Delta\lambda^2/2\lambda_p^2, \quad \Delta\lambda = |\lambda_s - \lambda_c|, \quad 2\lambda_p^{-1} = \lambda_s^{-1} + \lambda_c^{-1} \quad (2)$$

The quantity $\Delta\beta$ represents the phase mismatch between signal wave (wavelength λ_s) and converted wave (wavelength λ_c) owing to GVD parameter D_2, c is the speed of light in vacuum, and λ_p is the wavelength of the pump. By fitting these relations to the measured data, both γ and D_2 can be extracted.

The heterodyne pump-probe set-up is described in more detail in ref. 29. The measurement relies on a Spectra Physics OPAL optical parametric amplifier, which is synchronously pumped at a repetition rate of 80.42 MHz by a Tsunami Ti:sapphire mode-locked femtosecond laser. The pulses have a FWHM duration of 120 fs and a centre wavelength of 1,550 nm. Pump, probe and reference pulses are co-polarized (TE); probe and reference pulses are marked by distinct frequency offsets using acousto-optic modulators. After having passed the waveguide, the probe and the reference pulses are superimposed, and the beat signal is detected by a lock-in amplifier, hence revealing the pump-induced phase change $\Delta\varphi$ of the probe pulses.

In the measurements of Fig. 2b, a slot waveguide with height $h = 220$ nm, width $w = 216$ nm and slot width $w_{slot} = 157$ nm was used, whereas the strip waveguide

had a height $h = 220$ nm and width $w = 375$ nm. Both waveguides had a length $L = 4$ mm, and the average on-chip pump power was -1.2 dBm. For a waveguide of length L the phase change $\Delta\varphi$ is related to the pump-induced effective refractive index change Δn_e by $\Delta\varphi = -\Delta n_e 2\pi L/\lambda$. For the ultrafast Kerr responses shown in Fig. 2b (slot), the refractive index increased ($\Delta\varphi < 0$), whereas for the strip waveguide the presence of free carriers led to a pronounced slowly decaying decrease of the effective refractive index ($\Delta\varphi > 0$). The slow effect was barely visible in the case of the slot waveguide, because it was suppressed in two ways. First, because the light is confined to the cladding material of the slot waveguide, the number of TPA-generated free carriers is much smaller than in the strip waveguide. Second, the overlap of the slot waveguide mode with the silicon core is much smaller than for the strip waveguide—only 26% of the total optical power propagates within the silicon core, whereas 60% is guided in the nonlinear cladding and 14% in the silica buffer layer. The slot mode is hence only weakly affected by the carrier-induced decrease of the refractive index in the silicon core.

It can further be confirmed that the absence of slow carrier dynamics for the SOH slot waveguides is not caused by increased surface recombination owing to a larger surface-to-volume ratio. All waveguides were produced side by side on the same chip, and hence had identical recombination rates of free carriers at the surfaces. If d is the average distance that a carrier has to diffuse (random walk) until it reaches the surface, then the effective carrier lifetime is proportional to d^2. For the strip waveguide (width 375 nm) a carrier lifetime of $\sim$1.2 ns was measured. To a first approximation, the carrier lifetime of the slot waveguide (width 216 nm) should then be $1.2\ \text{ns}/(375^2/216^2) \approx 0.4$ ns, which would be clearly visible as a slowly decaying response in Fig. 2b. As this is not the case, we conclude that, indeed, the ultrafast nonlinear response originates from the nonlinear cladding.

Transmission experiment. For the transmission experiment, two synchronized Calmar mode-locked fibre lasers were used. The optical signals were detected with a u^2t 120 GHz photodiode, and the eye diagrams were recorded with an Agilent Infiniium digital communication analyser (DCA). Except for the intrinsic low-pass behaviour of the detector and the DCA, no further filtering of the electrical signal was performed for generating the eye diagrams in Fig. 3. The slot waveguide used for the demultiplexing experiment (height $h = 220$ nm, strip width $w = 212$ nm, slot width $w_{slot} = 205$ nm) had a propagation loss of $\alpha_{dB} = 1.5$ dB mm^{-1} and a fibre-chip coupling loss of $a_{cp} = 4.1$ dB per facet at 1,550 nm. The wavelength conversion efficiency in the present experiment was approximately -32 dB. There is still a huge potential for improvement by reducing the waveguide loss and by further increasing the nonlinearity of the waveguide[17].

The eye diagram of the converted wave disappears if either the pump or the signal wavelengths are blocked at the input of the device. By varying the delay between the pump and the signal, different tributaries of the optical time-division multiplexed (OTDM) data can be demultiplexed. Similar performance is found for the different tributaries. This confirms again that the recorded eye diagram is not caused by leakage through the filters. The extinction ratio of the demultiplexed eye diagram was $\sim$7.7 dB.

The noise in the converted eye diagram is predominantly caused by amplified spontaneous emission. It can be expected that the converted signal experiences retiming due to the periodic pump pulse sequence. The FWM demultiplexing scheme preserves both phase and amplitude information and is therefore transparent with respect to the modulation format.

Received 17 August 2008; accepted 13 February 2009; published online 15 March 2009

References

1. Tsuchizawa, T. *et al.* Microphotonics devices based on silicon microfabrication technology. *IEEE J. Sel. Top. Quantum Electron.* **11,** 232–240 (2005).
2. Lipson, M. Guiding, modulating, and emitting light on silicon—challenges and opportunities. *J. Lightwave Technol.* **23,** 4222–4238 (2005).
3. Popović, M. A. *et al.* Hitless-reconfigurable and bandwidth-scalable silicon photonic circuits for telecom and interconnect applications. Optical Fiber Communincation Conference (OFC'08), paper OTuF4 (OSA, 2008).
4. Bogaerts, W. *et al.* Compact wavelength-selective functions in silicon-on-insulator photonic wires. *IEEE J. Sel. Top. Quantum Electron.* **12,** 1394–1401 (2006).
5. Vlasov, Y. A., O'Bolye, M., Hamann, H. F. & McNab, S. J. Active control of slow light on a chip with photonic crystal waveguides. *Nature* **438,** 65–69 (2005).
6. Rong, H. *et al.* Low-threshold continuous-wave Raman silicon laser. *Nature Photon.* **1,** 232–237 (2007).
7. Espinola, R. L. *et al.* Raman amplification in ultrasmall silicon-on-insulator wire waveguides. *Opt. Express* **12,** 3713–3718 (2004).
8. Park, H. *et al.* A hybrid AlGaInAs–silicon evanescent amplifier. *IEEE Photon. Technol. Lett.* **19,** 230–232 (2007).
9. Fang, A. W. *et al.* Electrically pumped hybrid AlGaInAs–silicon evanescent laser. *Opt. Express* **14,** 9203–9210 (2006).
10. Van Thourhout, D. *et al.* A photonic interconnect layer on CMOS. European Conference on Optical Communications (ECOC'07), paper 6.3.1 (2007).
11. Koch, B. R., Fang, A. W., Cohen, O. & Bowers, J. E. Mode-locked silicon evanescent lasers. *Opt. Express* **15,** 11225–11233 (2007).
12. Park, H. *et al.* A hybrid AlGaInAs–silicon evanescent waveguide photodetector. *Opt. Express* **15,** 6044–6052 (2007).
13. Liao, L. *et al.* 40 Gbit/s silicon optical modulator for high-speed applications. *Electron. Lett.* **43,** 1196–1197 (2007).
14. Salem, R. *et al.* Signal regeneration using low-power four-wave mixing on silicon chip. *Nature Photon.* **2,** 35–38 (2008).
15. Kuo, Y.-H. *et al.* Demonstration of wavelength conversion at 40 Gb/s data rate in silicon waveguides. *Opt. Express* **14,** 11721–11726 (2006).
16. Hochberg, M. *et al.* Terahertz all-optical modulation in a silicon-polymer hybrid system. *Nature Mater.* **5,** 703–709 (2006).
17. Koos, C., Jacome, L., Poulton, C., Leuthold, J. & Freude, W. Nonlinear silicon-on-insulator waveguides for all-optical signal processing. *Opt. Express* **15,** 5976–5990 (2007).
18. Baehr-Jones, T. W., *et al.* Optical modulation and detection in slotted silicon waveguides. *Opt. Express* **13,** 5216–5226 (2005).
19. Hochberg, M. *et al.* Towards a millivolt optical modulator with nano-slot waveguides. *Opt. Express*, **15,** 8401–8410 (2007).
20. Brosi, J.-M. *et al.* High-speed low-voltage electro-optic modulator with a polymer-infiltrated silicon photonic crystal waveguide. *Opt. Express* **16,** 4177–4191 (2008).
21. Baehr-Jones, T. W. and Hochberg, M. J. Polymer silicon hybrid systems: A platform for practical nonlinear optics. *J. Phys. Chem. C* **112,** 8085–8090 (2008).
22. Almeida, V. R., Xu, Q., Barrios, C. A. & Lipson, M. Guiding and confining light in void nanostructure. *Opt. Lett.* **29,** 1209–1211 (2004).
23. Esembeson, B. *et al.* A high optical quality supramolecular assembly for third-order integrated nonlinear optics. *Adv. Mater.* **20,** 4584–4587 (2008).
24. Michinobu, T. *et al.* A new class of organic donor–acceptor molecules with large third-order optical nonlinearities. *Chem. Commun.* 737–739 (2005).
25. May, J. C., Biaggio, I., Bures, F. & Diederich, F. Extended conjugation and donor–acceptor substitution to improve the third-order optical nonlinearity of small molecules. *Appl. Phys. Lett.* **90,** 251106 (2007).
26. Koos, C. *et al.* Highly-nonlinear silicon photonics slot waveguide. Optical Fiber Communications Conference (OFC'08), postdeadline paper PDP25 (2008).
27. Leong, J. Y. Y. *et al.* A lead silicate holey fiber with $\gamma = 1860$ W^{-1} km^{-1} at 1550 nm. Optical Fiber Communications Conference (OFC'05), postdeadline paper PDP22 (2005).
28. Mägi, E. C. *et al.* Enhanced Kerr nonlinearity in sub-wavelength diameter As_2Se_3 chalcogenide fiber tapers. *Opt. Express* **15,** 10324–10329 (2007).
29. Vallaitis, T. *et al.* Slow and fast dynamics of gain and phase in a quantum dot semiconductor optical amplifier. *Opt. Express* **16,** 170–178 (2008).
30. Vallaitis, T. *et al.* Highly nonlinear silicon photonic slot waveguides without free carrier absorption related speed-limitations. Proc. 34rd European Conference on Optical Communication (ECOC'08), paper Th.2.D.6 (2008).

Acknowledgements

This work was supported in part by the DFG (German Research Foundation) Center for Functional Nanostructures (CFN), by the Initiative of Excellence of the University of Karlsruhe within a Feasibility Study of Young Scientists (FYS), the Karlsruhe School of Optics, and by the European project TRIUMPH (Transparent Ring Interconnection Using Multi-wavelength PHotonic switches, grant IST-027638 STP). We acknowledge support by the European Network of Excellence ePIXnet, including fabrication by ePIXfab (www.epixfab.eu), and by ASML Netherlands B.V., and we acknowledge equipment loan from Siemens Portugal and from Optoelectronics Research Centre (ORC) in Southampton, UK. I.B. and B.E. acknowledge partial support from the Commonwealth of Pennsylvania, Ben Franklin Technology Development Authority. F.D. and T.M. acknowledge support from the ETH research council.

Additional information

Reprints and permission information is available online at http://npg.nature.com/reprintsandpermissions/. Correspondence and requests for materials should be addressed to W.F. and J.L.